

# Consideration of locked-in stresses during backfill preparation

Ahmet Talha Gezgin<sup>a</sup> and Ozer Cincioğlu\*

*Department of Civil Engineering, Bogazici University, 34342 Bebek Istanbul, Turkey*

*(Received August 17, 2018, Revised May 28, 2019, Accepted May 30, 2019)*

**Abstract.** Soil strength and failure surface geometry directly influence magnitudes of passive earth thrust acting on geotechnical retaining structures. Accordingly, it is expected that as long as the shape of the failure surface geometry and strength parameters of the backfill are known, magnitudes of computed passive earth thrusts should be highly accurate. Building on this premise, this study adopts conventional method of slices for calculating passive earth thrust and combines it with equations for estimating failure surface geometries based on in-situ stress state and density. Accuracy of the proposed method is checked using the results obtained from small-scale physical retaining wall model tests. In these model tests, backfill was prepared using either air pluviation or compaction and different backfill relative densities were used in each test. When the calculated passive earth thrust magnitudes were compared with the measured values, it was noticed that the results were highly compatible for the tests with pluviated backfills. On the other hand, calculated thrust magnitudes significantly underestimated the measured thrust magnitudes for those tests with compacted backfills. Based on this observation, a new approach for the calculation of passive earth pressures is developed. The proposed approach calculates the magnitude and considers the influence of locked-in stresses that are the by-products of the backfill preparation method in the computation of lateral earth forces. Finally, recommendations are given for any geotechnical application involving the compaction of granular bodies that are equally applicable to physical modelling studies and field construction problems.

**Keywords:** model test; failure surface geometry; passive earth thrust; method of slices; locked-in stresses

## 1. Introduction

Construction of backfills might be required in various civil engineering projects for ground leveling, supporting or stabilization purposes. Methods used for backfilling varies based on the importance of the project and the intended purpose of the backfill. In addition to ordinary civil engineering projects, model backfills are prepared in laboratories for testing and research (Cho *et al.* 2018, Liu *et al.* 2018, Kazemi and Bolouri 2018, Khatri *et al.* 2017, Anil *et al.* 2017). In all these works, engineers and researchers noted that the method employed for backfill preparation influences the constituted properties of the backfill soils (Oda 1972, Miura and Toki 1982, Kuo and Frost 1996, Frost and Park 2003). Magnitudes of soil parameters such as cyclic shear strength or coefficient of lateral earth pressure change by whether pluviation is used or compaction is employed during backfilling effort (Ladd 1974, Hanna and Al-Romhein 2008). Several researchers investigated the effect of compaction on lateral earth pressure using simple analytical methods (Broms 1971, Ingold 1979, Potgieter 2017). According to these studies, soil sample preparation using compaction results in higher residual stresses. However, these stresses are direction dependent and can be persistent only in lateral directions

where the deformations are hindered (Chen and Fang 2008). Several studies are available in literature that investigates the influence of compaction effort on at rest and passive earth pressures (Hanna and Al Khoury 2005, Hanna and Al-Romhein 2008). According to Hanna and Al Khoury (2005), sample preparation via compaction procedure leads to additional stresses in the backfill which are locked-in. In their experimental study, Hanna and Al Khoury (2005) dealt with these stresses by considering them to induce overconsolidation ratio (OCR) in cohesionless soils. Similarly, Hanna and Al-Romhein (2008) following the approach of previous studies (Wroth 1972, Mayerhof 1976, Mayne and Kulhawy 1982) proposed an empirical equation to calculate the lateral earth pressure coefficient as a function of friction angle and OCR. However, unlike friction angle, OCR is not a variable that is easily calculated or measured. So, in order to better understand the development of passive earth pressures in cohesionless backfills and the influence of backfill preparation methods on their magnitudes, a physical model study was conducted.

As it is well known, passive earth thrust is a product of the resistance that develops along a failure plane that is created during shearing of the backfill. So, the premise of the current study is that passive earth thrust can be calculated as long as passive failure surface geometry, unit weight of the backfill material and shear resistance along the failure surface are known. To investigate this proposition, small scale physical model tests were conducted with cohesionless backfills under 1g conditions simulating passive failure state. The tests are repeated with different backfill densities and magnitudes of passive thrust

\*Corresponding author, Associate Professor

E-mail: [ozercincio@boun.edu.tr](mailto:ozercincio@boun.edu.tr)

<sup>a</sup>Ph.D. Candidate

E-mail: [ahmet.gezgin@boun.edu.tr](mailto:ahmet.gezgin@boun.edu.tr)

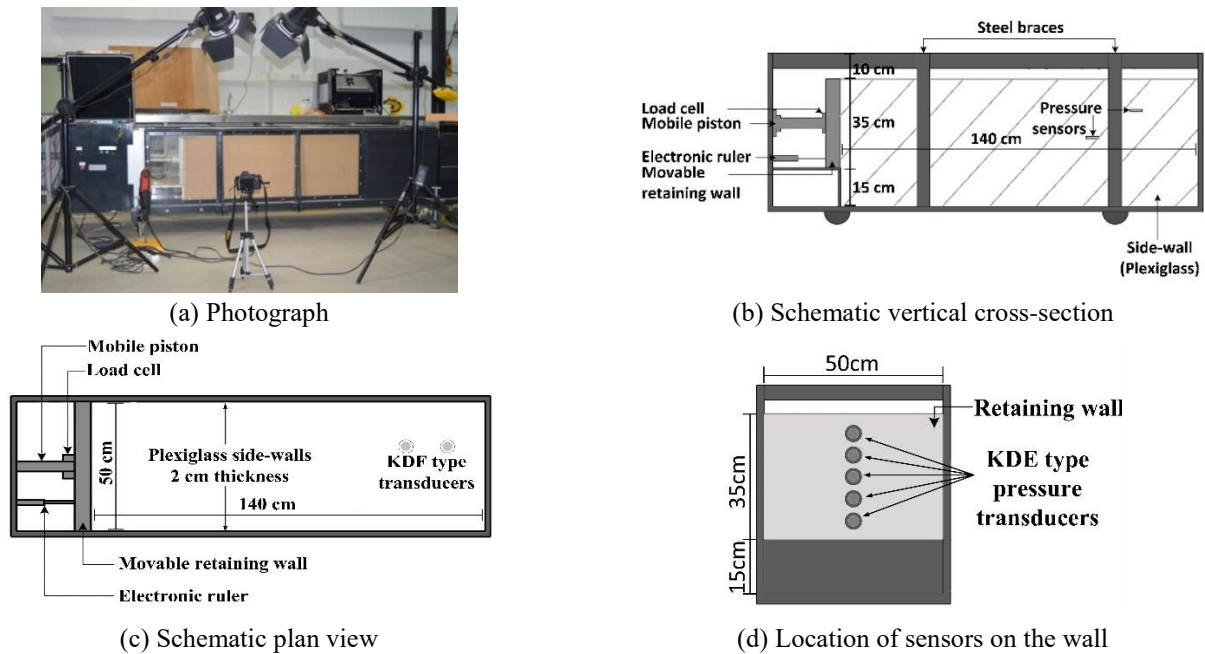


Fig. 1 Experimental set-up

are measured for each test. Necessary strength parameters relevant for the density and stress states of the backfill soils are calculated using specially calibrated empirical equations. Accordingly, this study uses method of slices (Rahardjo and Fredlund 1984, Zakerzadeh *et al.* 1999) on experimentally obtained and mathematically defined failure surfaces to calculate the magnitudes of passive thrust. For the purpose of identifying the failure surface, Particle Image Velocimetry (PIV) technique is used. Then, identified failure surfaces are quantified using the method proposed by Altunbas (2014). Finally, calculated thrust magnitudes using the method of slices are compared with the measured ones to understand the underlying mechanism of passive earth pressure for cohesionless soils. Comparison of model test results and calculated values showed that passive earth thrust is also dependent on the method of backfill preparation. The influence of backfill preparation method is quantified using the “locked-in stresses” concept. Finally, the results are discussed and the proposed method is compared with popular methods for calculating passive earth pressures.

## 2. Test setup

The 1g model used in this study to simulate passive backfill failure conditions consists of a testing tank, a movable model retaining wall, a sand pluviation system, a storage tank, a crane and a multi-channel data logger (Fig. 1(a)). The testing tank is 140, 60, and 50 centimeters in length, width and depth, respectively. The dimensions are shown in Fig. 1(b) and Fig. 1(c). The length of the model tank is selected long enough to ensure that the failure surface is not affected by the boundary at the far end. The sides of the testing tank are 50 mm thick Plexiglas allowing the observation and photographing of the deformations during testing. Owing to the high lateral pressures that are

imposed on the transparent walls, steel braces are used for reinforcing the thick Plexiglas to minimize possible deflections. Lateral wall deflections were measured before and after the tests to ensure that plane strain conditions prevail. Images of the backfill captured at different stages of model wall translation were later analyzed using PIV to identify the geometry of failure surfaces.

An aluminum plate capable of lateral translation acts as the model retaining wall. The plate has a rectangular cross-section that is 35 cm high and 50 cm wide. In order to minimize the adverse effects of the rigid boundary at the bottom, the plate is located 15 cm above the base of the test tank. It can move either in forward or backward directions. The horizontal movement of the wall is provided by an electrical motor with a maximum capacity of 3 Mg. Mechanical energy generated by the piston is transferred to the model wall through a piston. A load cell with a 5 kN capacity is mounted between the piston and the model wall to measure the lateral thrust necessary for translation type of motion. The range of movement capacity of the load cell is 150 mm. For the purpose of tracking the position of the model wall a linear variable displacement transducer (LVDT) which has an accuracy of 1% and a range between 0 mm and 300 mm is used. There are five sensitive soil pressure transducers mounted on the retaining wall model to measure lateral earth pressures acting on the model wall as shown in Fig. 1(d). These transducers are TML KDE type pressure transducers with a maximum capacity of 200 kPa and they are positioned vertically along the centerline of the model wall at equally spaced intervals. Pressure transducers are positioned to face in the direction of the backfill as depicted in Fig. 1(d). The input/output cable of each transducer comes from the center of the transducer body and passes through specially opened ducts within the model wall plate to be connected to the data acquisition box. In addition to these, two transducers are buried in the backfill during model preparation in order to measure the

magnitudes of vertical effective stresses at different depths. To increase the practicality of positioning these transducers within the backfill, TML KDF type transducers are preferred. The difference of KDF type pressure transducers is that the input/output cable connects to the transducer body from the side. As a result, positioning the transducer during model preparation becomes easier.

Data from the pressure transducers, load cell and LVDT are collected by means of a multi-channel data logger system (imc SPARTAN-1) which also provides an interface for monitoring the progress of the test. Imc SPARTAN-1 as a data acquisition system has 2 slots for up to 16 analog inputs. It can also handle an aggregate data collection rate of 400000 Sample/s with a maximum per channel sample rate of up to 500 Sample/s.

### 3. Properties of the testing sand

The soil used in the present study is a quartz-rich sand from Akpınar region near Istanbul. Sand that was transported to the laboratory was first washed, dried and then sieved. Gradation and shape characteristics of Akpınar Sand, as obtained from laboratory tests, are reported in Table 1. Gradation characteristics are based on the results of sieve analyses, whereas particle shape parameters were obtained following the methodology of Cho *et al.* (2006). Maximum and minimum void ratios of the testing sand were determined in accordance with the related standards (ASTM D-4253 and ASTM D-4254).

In order to consider the influences of the interfaces on the computed earth thrusts, it is necessary to know the plexiglas-sand and aluminum-sand interface friction angles. For this purpose, interface direct shear tests were conducted using special block samples of plexiglas and aluminum. As a result, plexiglas-sand interface friction angle was measured as 17° and aluminum-sand interface friction angle was measured as 19°. Variations in interface friction angles due to changes in pressure and backfill density are found to be insignificant.

In addition to the gradation and shape characteristics, strength and dilatant characteristics of the sand were investigated. As explained in the introduction section, this study focuses on the computation of passive earth thrust using the method of slices for known and mathematically defined failure surfaces. However, in order to know the strength parameters relevant for the backfill sand experimentally calibrated empirical relationships are used. The underlying reason for this approach is that the friction angle varies with changes in density and stress state. Since it is not possible to obtain samples of the cohesionless soils or test them in-situ for direct measurement of friction angle, numerous laboratory tests were conducted to mathematically define the variations in peak friction angle ( $\phi'_p$ ) and dilatancy angle ( $\psi_p$ ). First of all, the magnitude of  $\phi'_p$  will be calculated as a function of  $\psi_p$  using the empirical relationship defined by Bolton (1986) as shown in Eq. (1).

$$\phi'_p = \phi'_c + r\psi_p \quad (1)$$

Here,  $\phi'_c$  is the critical state friction angle and  $r$  is an empirical line-fitting parameter.  $\psi_p$  in Eq. (1) is dependent

Table 1 Basic properties of the tested sand

Property	Value
Classification	Poorly Graded (SP)
Max. void ratio ( $e_{\max}$ )	0.87
Min. void ratio ( $e_{\min}$ )	0.58
Uniformity coefficient (Cu)	1.23
Coefficient of gradation (Cc)	0.97
Specific gravity (Gs)	2.63
Average sphericity ( $S_{\text{ave}}$ )	0.7
Average roundness ( $R_{\text{ave}}$ )	0.5

Table 2 Mechanical properties of Akpınar Sand

Parameter	Value
Critical state friction angle, $\phi'_c$ (°)	33.8
Influence of $\psi_p$ on $\phi'_p$ for axisymmetric conditions, $r_{tx}$	0.39
Influence of $\psi_p$ on $\phi'_p$ for plane-strain conditions, $r_{ps}$	0.66
Stress-based dilatancy constant, $\alpha_\psi$	-0.066
Density-based dilatancy constant, $m_\psi$	0.64

on the in-situ stress state and relative density which is expressed as (Cinicioglu and Abadkon 2015)

$$\tan \psi_p = \alpha_\psi \left( \frac{p'_i}{p_a} \right) + m_\psi I_D \quad (2)$$

where  $p'_i$  is the preshear mean effective stress,  $p_a$  is the standard atmospheric pressure at sea level, and  $I_D$  is the relative density. Accordingly,  $\alpha_\psi$  and  $m_\psi$  are unit-independent empirical line-fitting parameters that define the variations in  $\psi_p$  due to changes in preshear stress state, preshear density and the expected stress path to be followed of the soil, respectively. In this study, magnitudes of preshear stress state and density are known and the stress path is predefined. In order to obtain the magnitudes of soil and stress path specific empirical constants ( $\alpha_\psi$  and  $m_\psi$ ), several consolidated-drained triaxial tests were conducted on reconstituted samples of Akpınar sand at different combinations of  $p'_i$ - $I_D$ . Previous researchers have noticed the independence of  $\psi_p$  from imposed symmetry conditions such as plane strain or axial symmetry (Bolton 1986; Schanz and Vermeer 1996). Thus, even though  $\alpha_\psi$  and  $m_\psi$  are dependent on the followed stress path, they are not affected by the changes in symmetry conditions. Therefore, empirical constants  $\alpha_\psi$  and  $m_\psi$  obtained from triaxial tests will also be valid for plane strain conditions. However,  $r$  values obtained from the results of triaxial tests are relevant for axisymmetric conditions but will not be applicable to plane strain conditions as in the case of the retaining wall model. Therefore, even though  $\phi'_c$  and  $\psi_p$  are directly suitable for the plane-strain conditions,  $\phi'_p$  cannot be calculated by directly inserting the  $r$  value obtained under axisymmetric conditions into Eq. (1). This is a consequence of the fact that  $\phi'_p$  values of triaxial and plane strain tests slightly differ (Hanna 2001, Schanz and Vermeer

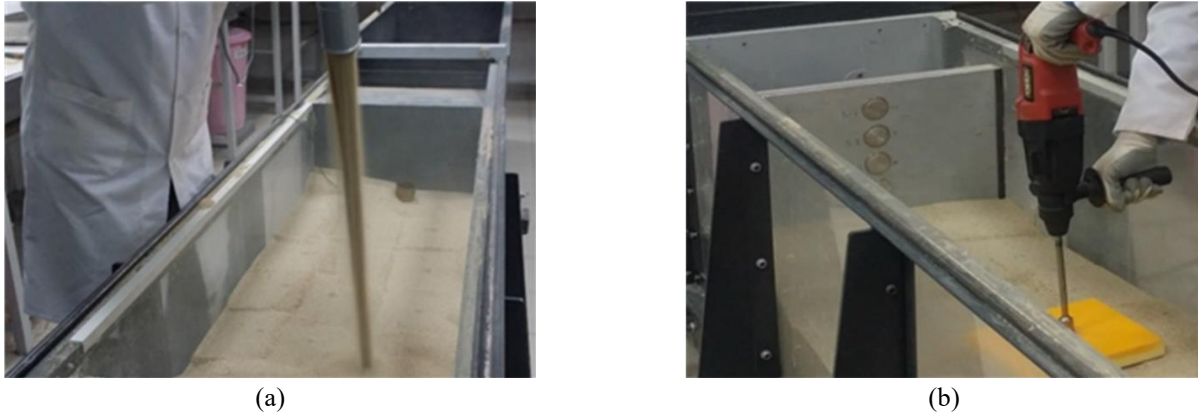


Fig. 2 Placement of the sand by (a) pluviation method and (b) the compaction method

1996). Hence,  $\phi'_p$  values relevant for plane-strain conditions were calculated from  $\phi'_p$  values measured in triaxial tests using the method proposed by Nanda and Patra (2015)

$$\phi'_p = \phi'_T \left[ 1.5 \times \left( \frac{1 - K_{\phi T}}{1 - 0.19e^{[1.667 \times K_{\phi T}]}} \right) \right] \quad (3)$$

where  $\phi'_p$  is the plane strain peak friction angle,  $\phi'_T$  is the triaxial peak friction angle and  $K_{\phi T}$  is the ratio of  $\phi'_c$  to  $\phi'_T$ . Once  $\phi'_p$  values relevant for plane-strain conditions are calculated using Eq. (3), they are plotted against corresponding  $\psi_p$  values. The resulting linear relationships zero-intercept corresponds to  $\phi'_c$  (when  $\psi_p=0$ ) and slope corresponds to  $r$  value that is suitable for plane-strain conditions. Hence, the mechanical parameters of Akpinar Sand that are suitable for plane-strain conditions are given in Table 2.

Alternative to using Eq. (2) proposed by Cinicioglu and Abadkon (2015), it is equally acceptable to use Eq. (4) proposed by Bolton (1986) to predict the value of  $\psi_p$ .

$$\psi_p = \frac{A_\psi}{r} \left[ I_D \left( Q - \ln \frac{100p'_f}{p_a} \right) - R \right] \quad (4)$$

In Eq. (4),  $Q$ ,  $R$ , and  $r$  are empirical line-fitting parameters.  $A_\psi$  is a constant and its value is 3 under axisymmetric conditions and 5 under plane strain conditions (Bolton 1986). The necessary values of the parameters of Bolton (1986) equation for Akpinar Sand are given in Altunbas *et al.* (2017).

#### 4. Testing methodology

Small-scale retaining wall model tests were conducted using the test set-up described in the previous sections. Since the tests are conducted without the application of surcharge at 1g using dry Akpinar sand and the dimensions of the model are fixed, mechanical properties of the backfill such as friction and dilatancy angles vary with the relative density of the backfill. Thus, the goal was to conduct each test using a different homogeneous backfill density. As explained above, two different methods of backfill preparation were used. The first method was the dry pluviation of sand from a fixed height (Fig. 2(a)).

Accordingly, sand was pluviated from a fixed height that was determined based on test specific target relative density. The falling height was maintained constant by slowly raising the pluviation tube. The height of pluviation was determined based on the results of the preliminary tests which were designed to investigate the relationship between pluviation heights and achieved relative density for Akpinar Sand. During the process of backfill preparation, several density cans were placed in the backfill following a staggered scheme in the vertical direction and within the portion of the model tank that is not affected by the deformations in the backfill during the tests. After the completion of each model test, these density cans were carefully retrieved to verify whether the desired relative density was achieved homogeneously. Only the tests with homogeneous backfills were deemed successful and considered in the analyses. However, the maximum density that can be achieved using only pluviation is rather limited, therefore an alternative method of model backfill preparation was developed. The alternative method of backfill preparation uses both air pluviation and compaction to achieve greater backfill densities. In the first stage of the alternative method of backfill preparation, dry pluviation is used in which the sand is spread in the model box in layers by raining through a hopper. Each layer was then compacted using an electrical hand compactor for models that require denser backfills as shown in Fig. 2(b). The degree of density of the backfill can be adjusted by adjusting the compaction time. Depth of individual layers were accounted for by varying the layer thicknesses based on their relative positions along the depth of the model box. This method required operator skill and experience and uniformity of the backfill with depth was checked using the results of density cans. Later, the results of those tests with homogeneous backfills were used in the analysis stage as achieving uniformity is critical for the calculations of the magnitudes of  $\phi'_p$  and  $\psi_p$ .

During backfill preparation, soil pressure transducers were placed in the backfill with their sensing surfaces facing upwards. They were located at different depths to monitor the variations in the magnitude of vertical effective stresses. These transducers were positioned close to the far end of the model box away from the model wall in order to prevent the possible interference of the transducers with the

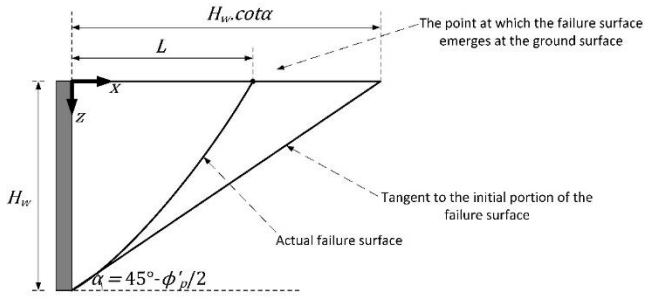


Fig. 3 Comparison of the actual failure surface with the linear failure surface and the definition of the coordinate system

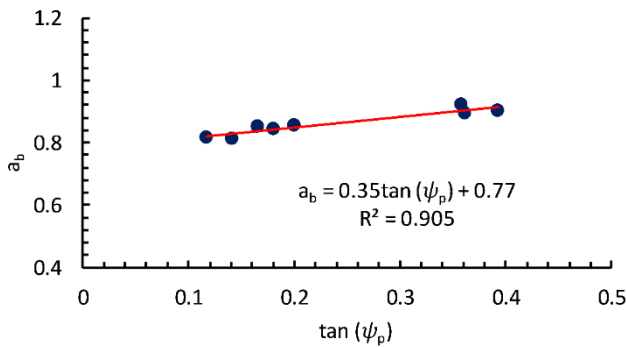


Fig. 4  $a_b$ - $\tan(\psi_p)$  relationship obtained using the data gathered from retaining wall model study for passive cases

shear bands. All the transducers used in the model tests were calibrated prior to the tests. Following the preparation of the backfill, recording and illumination devices were placed for capturing high quality images of the tests. The model was illuminated using two standing adjustable LED light sources which have a power of 10 watts and a colour temperature of  $5600 \pm 300$  K as shown in Fig. 1(a) to improve the quality of the images captured by a digital camera that has a 24.2 megapixel complementary metal oxide semiconductor sensor. The digital camera used for capturing images at consecutive stages of the test was positioned such that the axis of its lens coincides with the center of the expected strain field. In addition, the position and the height of the camera were fixed before the planned tests and they were never changed throughout the period of testing. The camera can record images to the memory card at a rate of 4 images/s and the memory card capacity is 32 GB. Therefore, the rate of continuous image capturing was fixed to 2 images/s. This way all stages of the test could be photographed at the fixed rate of wall translation throughout the entire duration of the tests without filling the entire capacity of the memory card. Additionally, in order to prevent any vibrations camera was controlled remotely.

Data collection was initiated prior to the start of the test to learn about the initial conditions. Similarly, initial state of the backfill was photographed to be used as the reference frame during image analyses.

Afterwards, the model tests were started by translating the wall horizontally towards the model backfill at a constant speed of 3 mm/s. The speed of wall translation was selected to recreate the same rate effects that the sand

samples experience during the shearing phase of the triaxial tests from which the parameters in Table 2 were obtained. The tests were continued until the state of passive failure of the backfill was significantly exceeded.

Captured images were used for the identification of the deformation field using PIV method. It is a digital image-based surface displacement measurement technique that examines the differences between a reference image and a sequence of deformed images. Accordingly, PIV tracks the variations in the quantity of light by comparing all of the images of planar soil deformation taken during the test. Consequently, evolution of the displacement field can be monitored. Finally, strains can be calculated through gradients of determined displacements. In this study, PIV analyses were conducted using the software GeoPIV (White *et al.* 2003). GeoPIV is a MATLAB based software that is specifically crafted for geotechnical applications.

## 5. Quantification of the geometry of passive failure surface

As explained in the previous sections, this study combines method of slices with accurately quantified failure surfaces to calculate the magnitudes of passive earth thrust. Therefore, it is necessary to mathematically define the passive failure surface geometry based on mechanical properties of the backfill used. This is achieved by quantifying the failure surfaces that are identified using PIV method following the approach (Altunbas 2014) developed for the quantification of active failure surfaces. Altunbas (2014) showed that passive failure surfaces have parabolic forms and thus their geometries can be quantified using second order parabolic functions as shown in Eq. (5).

$$z = ax^2 + bx + c \quad (5)$$

The constants of the second order parabolic function ( $a, b$  and  $c$ ) can be solved by defining the boundary conditions. These boundary conditions are as follows: failure surface starts at the bottom of the retaining wall, its initial inclination is  $\alpha = 45^\circ - \phi'_p/2$ , and the horizontal distance between the model wall and the point at which the failure surface emerges is

$$L = a_b H_w \cot(\alpha) \quad (6)$$

where  $a_b$  is the ratio of the horizontal distance from the wall to the actual point at which failure surface emerges at the ground surface ( $L$ ) and the distance that is measured horizontally between the wall and the point at which the tangent to the initial portion of the failure surface emerges at the backfill surface ( $H_w \cot(\alpha)$ ) as illustrated in Fig. 3. Following the suggestion of Altunbas (2014), it has been shown that  $a_b$  is a linear function of  $\psi_p$  when the results of all passive tests are collected as shown in Fig. 4. Inserting the empirical  $a_b - \tan \psi_p$  relationship for Akpinar Sand shown in Fig. 4 into Eq. (6), the horizontal distance between the model wall and the point at which the failure surface emerges ( $L$ ) can be calculated empirically as a function of peak dilatancy angle ( $\psi_p$ ) as given in Eq. (7).

$$L = [(0.3525 \tan \psi_p) + 0.777] \times H_w \cot(\alpha) \quad (7)$$

Using the boundary conditions explained above, the constants  $a$ ,  $b$ , and  $c$  can be identified as shown in Eqs. (8), (9), and (10).

$$a = \left[ \frac{(a_b - 1)}{(a_b^2 H_w)} \right] \tan^2(\alpha) \quad (8)$$

$$b = -\tan(\alpha) \quad (9)$$

$$c = H_w \quad (10)$$

The second order parabolic equation for the passive failure surface can be obtained by inserting the constants given in Eqs. (8), (9), and (10) into Eq. (5).

$$z = \left( \left[ \frac{(a_b - 1)}{(a_b^2 H_w)} \right] \tan^2(\alpha) \right) x^2 - \tan(\alpha)x + H_w \quad (11)$$

In this study, the quantification method proposed by Altunbas *et al.* (2017) is adapted to passive failure conditions. Using the empirical  $a_b - \tan \psi_p$  relationship as defined in Fig. 4 and solving the second order parabolic equation for boundary conditions, resulting empirical equation for calculating the geometry of passive failure surface as developed for the backfill Akpinar Sand in this study is obtained as given in Eq. (12).

$$z = \left[ \left( \frac{(0.3525 \tan \psi_p) - 0.223}{((0.3525 \tan \psi_p + 0.777)^2 H_w)} \right) \times \left( \tan \left( 45 - \frac{\phi'_p}{2} \right) \right)^2 \right] x^2 - \tan \left( 45 - \frac{\phi'_p}{2} \right) x + H_w \quad (12)$$

Here in Eq. (12),  $H_w$  is the height of the wall,  $z$  is the depth from ground surface, and  $x$  is the horizontal distance of the point from the model wall as shown in Fig. 3.

## 6. The formulation

In this study, passive thrust is calculated using a limit equilibrium approach. For this purpose, force equilibrium is defined for the soil mass enclosed within boundaries defined by the model wall, backfill surface and the failure surface. The forces acting on the soil mass are shown in Fig. 5. These are the forces exerted by the wall ( $P$ ), the weight of the soil mass within the failure zone ( $W$ ), interface friction between the backfill and the plexiglass ( $F_s$ ), the normal and shear forces between the failing wedge and surrounding soil ( $N$  and  $S_m$ ) as shown in Fig. 5.

In order to calculate the passive thrust, the soil mass above the failure surface is divided into slices having equal widths. Then force equilibrium equations in horizontal and vertical directions are defined for each slice. The shear force acting on the base of each slice is calculated in accordance with the Mohr-Coulomb failure criterion shown in Eq. (13)

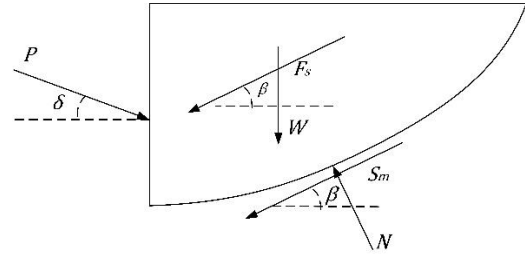


Fig. 5 Forces acting on soil mass in passive failure state

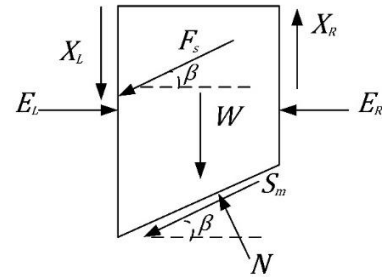


Fig. 6 Forces acting on each slice

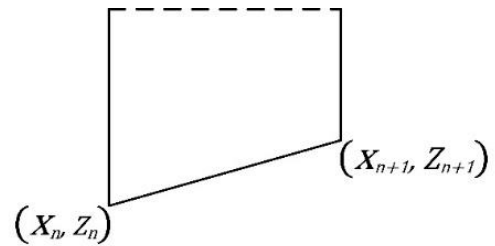


Fig. 7 The coordinates of the base corners of  $n^{\text{th}}$  slice

$$\tau = c' + \sigma'_n \tan \phi' \quad (13)$$

where  $\tau$  is the shear strength at failure,  $c'$  is the effective cohesion at failure,  $\phi'$  is the effective internal friction angle, and  $\sigma'_n$  is the normal effective stress at failure. Forces that are assumed to act on each slice are illustrated in Fig. 6.

In Fig. 6,  $W$  is the weight of the slice,  $N$  and  $S_m$  are the normal and shear forces acting on the base of the slice,  $F_s$  is the frictional force that develops at the interface between the backfill and the plexiglas surfaces,  $E_L$  and  $E_R$  are the normal interslice forces acting on the sides,  $X_L$  and  $X_R$  are the shear interslice forces on the sides of the slice. The angle between the tangent to the midpoint of the base of the slice and horizontal is shown by  $\beta$ . Clearly  $\beta$  varies with position which should be considered in the computations.

The weight of the slice is computed by product of the volume of the slice ( $V$ ) and the unit weight of the backfill ( $\gamma$ ) as shown in Eq. (14).

$$W = V \times \gamma \quad (14)$$

Therefore, the volume of the slice ( $V$ ) is calculated using Eq. (15) based on the coordinate values of the base corners of the  $n^{\text{th}}$  slice shown in Fig. 7.

In Fig. 7,  $z_n$  is the depth from ground surface,  $x_n$  is the horizontal distance to the model wall and  $B$  is the

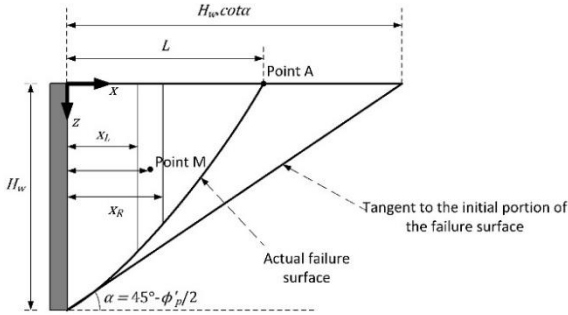


Fig. 8 The assumed common length for right and left sides of the slice

width of the testing tank that is equal to 50 centimeters. The value of  $z_n$  can be calculated as a function of  $x_n$  using Eq. (12).

$$V = \frac{(z_n + z_{n+1}) \times (x_{n+1} - x_n)}{2} \times B \quad (15)$$

The other force acting on the slice is the interface frictional force that develops between the plexiglass and the backfill on both sides of the testing tank. As there is no deformation in the direction transverse to the direction of wall movement, it is assumed at rest conditions prevail when calculating the earth pressure acting on the plexiglass side walls. Then, using Eq. (16), the total frictional force  $F_S$  developing on both sides of  $n^{\text{th}}$  slice can be calculated.

$$F_S = 2 \times \left[ \frac{1}{4} \times \gamma \times (z_n^2 + z_{n+1}^2) \times (x_{n+1} - x_n) \times K_o \times \tan \theta \right] \quad (16)$$

Here,  $K_o$  is lateral earth pressure coefficient at rest, and  $\theta$  is the interface friction angle between the plexiglass and the backfill.

In order to calculate the normal force acting on the base of each slice, vertical and horizontal force equilibrium equations are written as shown in Eqs. (17)-(18), respectively.

$$W + X_L - X_R + S_m \times \sin \beta - N \times \cos \beta + F_S \times \sin \beta = 0 \quad (17)$$

$$E_L - E_R - S_m \times \cos \beta - N \times \sin \beta - F_S \times \cos \beta = 0 \quad (18)$$

Shear force magnitudes mobilized on the bases of each slice can be identified following the form in Eq. (13) as shown in Eq. (19).

$$S_m = N \times \tan \phi'_p \quad (19)$$

Substituting Eq. (19) into Eqs. (17) and (18) and dividing Eq. (17) by Eq. (18) yields Eq. (20).

$$\frac{X_R - X_L}{E_R - E_L} = \frac{W + N \times (\tan \phi'_p \times \sin \beta - \cos \beta) + F_S \times \sin \beta}{-N \times (\tan \phi'_p \times \cos \beta + \sin \beta) - F_S \times \cos \beta} \quad (20)$$

In order to solve for  $N$ , an assumption is necessary regarding the  $(X_R - X_L)/(E_R - E_L)$  ratio. Therefore, the assumption made by Fan (1983) is adopted defining the relationship between the vertical and horizontal components of interslice forces as given below

$$\frac{X_R - X_L}{E_R - E_L} = -(\tan \delta) \frac{(L - x)}{L} \quad (21)$$

where  $\delta$  is the backfill-model wall interface friction angle. In order to render the quantification of  $(X_R - X_L)/(E_R - E_L)$  possible, the horizontal distances of the left and right sides of the slices from Point A (the point at which the failure surface emerges at the ground surface) are assumed to be equal to each other ( $x_L = x_R$ ). Thus for each slice,  $x$  in Eq. (20) becomes equal to the horizontal distance between Point A and the horizontal midpoint of the considered slice (Point M) shown in Fig. 8.

Accordingly, in order to calculate the normal force acting on the base of each slice, Eqs. (20) and (21) are combined

$$\begin{aligned} N &= \left[ F_S \times \left( \sin \beta - \frac{\cos \beta \times \tan \delta \times (L - x)}{L} \right) + W \right] \\ &\times \left[ \left( \cos \beta - \tan \phi'_p \times \sin \beta \right. \right. \\ &\left. \left. + \frac{\tan \delta \times (\sin \beta + \tan \phi'_p \times \cos \beta) \times (L - x)}{L} \right) \right]^{-1} \end{aligned} \quad (22)$$

Horizontal distance between the wall and the point where the failure surface emerges on the backfill surface ( $L$ ) and the slope angle of the base of each slice ( $\beta$ ) in Eq. (22) are dependent on the magnitude of  $\psi_p$  since they are based on the relationships defined in Eqs. (7) and (23). For calculating  $\beta$  of each slice, coordinates of the base of the slices as shown in Fig. 7 are calculated using Eq. (12). Then using the notation shown in Fig. 7 for the  $n^{\text{th}}$  slice, tangent of  $\beta$  for the  $n^{\text{th}}$  slice can be obtained using Eq. (23).

$$\tan \beta = \frac{z_n - z_{n+1}}{x_{n+1} - x_n} \quad (23)$$

In order to calculate  $\tan \beta$  as a function of  $\psi_p$  for Akpınar Sand, Eq. (12) is substituted into Eq. (23) as shown in Eq. (24).

$$\begin{aligned} \tan \beta = & \left[ \left( \frac{(0.353 \tan \psi_p) - 0.22}{(0.353 \tan \psi_p + 0.78)^2 H_w} \right) \times \left( \tan \left( 45 - \frac{\phi'_p}{2} \right) \right)^2 \right. \\ & \times (x_n^2 - x_{n+1}^2) \\ & \left. - \tan \left( 45 - \frac{\phi'_p}{2} \right) \times (x_n - x_{n+1}) \right] \\ & \times [(x_{n+1} - x_n)^{-1}] \end{aligned} \quad (24)$$

In order to compute the magnitude of passive earth thrust ( $P_p$ ) acting on the wall as shown in Fig. 5, all the forces acting on the slices except the interslice forces ( $X_R$ ,  $X_L$ ,  $E_R$ , and  $E_L$ ) are considered. The resulting equation of overall force equilibrium in the horizontal direction for the case of zero cohesion is shown in Eq. (25).

$$P_p \times \cos \delta = \sum N \sin \beta + \sum S_m \cos \beta + \sum F_S \cos \beta \quad (25)$$

In Eq. (25), the normal force ( $N$ ) and the frictional force ( $F_S$ ) are calculated using Eqs. (22) and (16), respectively. Likewise, the base slope angle of each slice ( $\beta$ ) is computed as shown in Eq. (24). On the other hand, the shear force

( $S_m$ ) is calculated using the relationship between the normal force ( $N$ ) and the shear force ( $S_m$ ) for cohesionless soils given in Eq. (19).

## 7. Calculation of passive earth thrust with the mathematically defined failure surfaces

The premise of this study is that passive thrust can be calculated with high accuracy using limit equilibrium methods as long as the associated backfill failure plane and the associated strength parameters are known. To investigate the validity of this proposition, small scale physical model tests were conducted simulating passive failure state in cohesionless soils. To evaluate the validity, the preceding proposition, actual failure surfaces were identified using PIV method. Then, the adopting the method proposed by Altunbas *et al.* (2017), geometries of the failure surfaces were quantified as functions of  $\psi_p$ . Additionally, backfill strength parameters are calculated using backfill relative density and initial stress state by combining Eq.(1) (Bolton, 1986) and Eq. (2) (Cinicioglu and Abadkon, 2015). Necessary formulation is presented in detail in previous sections. It is necessary to use these equations since the values of  $\phi'_p$  and  $\psi_p$  vary as functions of density and stress state and sampling of dry cohesionless soil is not possible.

During the experimental program eight model tests were conducted. Backfill soils were prepared at different relative densities following the procedure defined in the testing methodology section. Accordingly, five model tests for which lower relative density backfills were targeted, only air pluviation method was used. However, for three model tests that required denser backfills, sand was compacted following the procedure defined in testing methodology. Altunbas (2014) showed that failure surface geometry is not influenced by the method of backfill preparation and it is only a function of  $\psi_p$ . The evidence of this study supported this suggestion as illustrated in Fig. 4. Moreover, as Cinicioglu and Abadkon (2015) pointed out,  $\psi_p$  is not influenced by OCR of the sample. Therefore, model preparation technique influences neither  $\phi'_p$  nor  $\psi_p$ . Following the completion of model tests, passive earth thrust magnitudes were calculated using Eq. (25). Then, calculated passive thrust magnitudes were compared with the measured thrusts. Measured passive earth thrust is calculated from the earth pressure distribution acting on the model wall at the instance of peak failure as measured by the five pressure transducers mounted along the vertical midsection of the model wall (Fig. 1(d)). Comparisons of the measured and calculated passive earth thrust magnitudes are shown in Fig. 9.

When Fig. 9 is examined, it is noticed that the calculated and measured thrust magnitudes are in good agreement for the tests on backfills prepared by pluviation. On the other hand, for the tests on backfills that were prepared by applying compaction, the calculated passive thrust magnitudes are significantly less than the measured ones.

It is known that compaction of backfills increases their overconsolidation ratio (OCR) (Hanna and Al Khoury

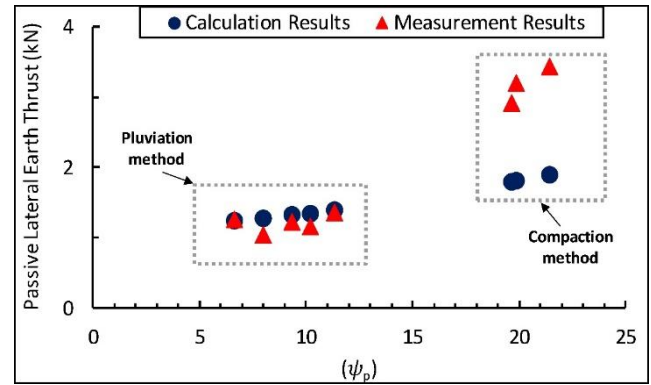


Fig. 9 The relationship between dilatancy angle and passive lateral earth thrusts according to calculation and measurement results

2005). On the other hand,  $\psi_p$  and  $\phi'_p$  are functions of relative density and mean effective stress (Bolton 1986, Schanz and Vermeer 1996, Cinicioglu and Abadkon 2015, Chakraborty and Salgado 2010). Therefore, values of  $\psi_p$  and  $\phi'_p$  do not change with OCR and they can be directly calculated as long as the variations in  $I_D$  and  $p'_i$  are considered in Eq. (2). Then, as long as the correct failure surface and strength parameters are known, the only reason for the difference between the calculated and measured passive thrust magnitudes might be the effective stresses present, but not accounted for in the backfill.

## 8. Locked-in stress concept

When air pluviation is used for preparing model backfill, soil grains arrange themselves within the mass without any significant exposure to granular deformation, neither elastic nor plastic. Thus, the grains can find a suitable position within the soil skeleton as illustrated in Fig. 10(a). However, when using compaction is considered for backfill preparation, the compaction effort forces the soil grains in between other grains in order to increase dry unit weight. Since the voids are small in comparison to the size of grains, grains push each other under the force of vibration. So, the grains deform. When the post compaction grain sizes are evaluated by sieving, it is observed that this deformation is primarily elastic. The elastic grain deformation generates normal forces at the points of intergranular contact as illustrated in Fig. 10(b). As the induced elastic compression results in additional normal forces between grains, in return these additional forces create frictional forces between the grains. Resulting increase in the frictional resistance creates a stabilizing effect and the grains cannot return their initial positions even after the compaction process is completed. Due to this, the compacted soil becomes denser as illustrated in Fig. 10(b). The role of the granular skeleton in this mechanism is similar to the case of compressed springs. Elastic deformations at the granular level increases the intergranular normal forces, which in turn increases the lateral earth pressure coefficient at rest ( $K_0$ ). Hence, these additional stresses are referred to as locked-in stresses. This

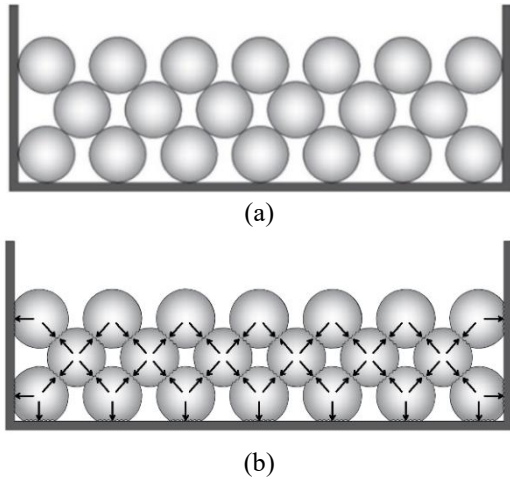


Fig. 10 Placement of the sand by (a) pluviation method and (b) the compaction method

phenomenon was observed and referred to as locked-in stresses by different researchers (Rehman and Broms 1972, Sherif and Mackey 1977, Duncan and Seed 1986, Hanna and Al Khoury 2005, Hanna and Al-Romhein 2008).

The magnitude of locked-in stresses can be identified as the difference between the mean effective stresses at the compacted state and the pluviated state (or normally compressed state) as shown in Eq. (26)

$$I_{\sigma} = (p'_i)_{comp} - (p'_i)_{nc} \quad (26)$$

where  $(p'_i)_{comp}$  is the initial mean effective stress in the compacted cohesionless soil and  $(p'_i)_{nc}$  is the initial mean effective stress in the pluviated cohesionless soil. Thus, the effective stresses at two different states should be determined as the difference results from the locked-in stresses generated during the compaction process. The mean effective stress can be calculated using Eq. (27).

$$p'_i = \frac{\sigma'_{vc} + 2 \times \sigma'_{hc}}{3} = \frac{\sigma'_{vc} \times (1 + 2K_0)}{3} \quad (27)$$

In Eq. (27),  $\sigma'_{vc}$  and  $\sigma'_{hc}$  are the vertical and horizontal effective stresses, respectively.  $K_0$  corresponds to the coefficient of lateral earth pressure at rest. It is possible to calculate the value of  $K_0$  for normally consolidated state ( $(K_0)_{nc}$ ) either by using the readings of the pressure sensors at the at rest state or by using Eq. (28) (Jaky 1944)

$$p'_i = \frac{\sigma'_{vc} + 2 \times \sigma'_{hc}}{3} = \frac{\sigma'_{vc} \times (1 + 2K_0)}{3} \quad (28)$$

where  $\phi'_p$  is calculated using Eqs. (1) and (2). Whether  $(K_0)_{nc}$  is calculated using sensor readings or using Eq. (28), computed magnitudes of  $(p'_i)_{nc}$  do not differ practically for pluviated backfills. Therefore, the magnitude of  $I_{\sigma}$  in Eq. (26) is practically zero for loose backfills. However, this is not the case when compacted backfills are considered as Eq. (28) is not applicable to compacted soils. Therefore  $(p'_i)_{comp}$  must be calculated using pressure sensor readings. On the other hand, in order to calculate  $I_{\sigma}$  for compacted backfills, it is necessary to be able to predict

the possible value of  $(p'_i)_{nc}$  as if the dense state of the soil is achieved just by particle rearrangement in the absence of loading and unloading that regenerates locked-in stresses. Then  $\phi'_p$  which is a function of stress state and density through Eqs. (1) - (2), and hence independent of OCR (Bolton, 1986); Schanz and Vermeer 1996; Cinicioglu and Abadkon 2015; Chakraborty and Salgado 2009), can be calculated for this assumed dense and supposedly normally consolidated state. Using the calculated  $\phi'_p$  in Eq. (28),  $(K_0)_{nc}$  is computed. Then, using the knowledge of backfill density, the magnitude of  $\sigma'_{vc}$  for the supposed normally compressed state is determined. Inserting  $\sigma'_{vc}$  and  $(K_0)_{nc}$  into Eq. (27),  $(p'_i)_{nc}$  is obtained. Finally, using  $(p'_i)_{nc}$  from Eq. (27) and  $(p'_i)_{comp}$  determined from pressure sensor readings,  $I_{\sigma}$  is calculated using Eq. (26).

As expected, the presence of locked-in stresses ( $I_{\sigma} > 0$ ) results in higher confining pressures in cohesionless soils. Ostensible influence of locked-in stresses on strength resembles cohesion effect. Following the custom practice when the strength of the soil is calculated as a function of vertical effective stresses, the increase in strength due to locked-in stresses is overlooked and the deviation between the measured and calculated strength magnitudes is regarded as cohesion. However, the difference is a resultant of purely frictional behavior. Locked-in stresses increase the normal intergranular contact stresses, which in turn increases frictional resistance. Then the magnitude of this surplus strength must be equal to locked-in stress times tangent of the peak friction angle. Accordingly, shear resistance that develops at the base of slice of compacted cohesionless soil can be calculated using Eq. (29)

$$S_m = (S \times B \times I_{\sigma} + N) \times \tan \phi'_p \quad (29)$$

where  $S$  is the length of the base of the slice,  $B$  is the width of the testing tank and  $I_{\sigma}$  is the locked-in stress at the base of the slice. The method proposed for the calculation of the normal force acting on the base of each slice (Eq. (22)) is modified considering the influence of the locked-in stresses as shown in Eq. (30).

$$\begin{aligned} & N \\ &= \left[ (F_S + I_{\sigma} \times \tan \phi'_p \times S \times B) \right. \\ & \times \left( \sin \beta - \frac{\cos \beta \times \tan \delta \times (L - x)}{L} \right) + W \left. \right] \\ & \times \left[ \left( \cos \beta - \tan \phi'_p \times \sin \beta \right. \right. \\ & \left. \left. + \frac{\tan \delta \times (\sin \beta + \tan \phi'_p \times \cos \beta) \times (L - x)}{L} \right)^{-1} \right] \end{aligned} \quad (30)$$

With the proposed method, passive lateral earth thrust that involve the locked-in stress effect is computed using Eq. (25) in which the shear and normal forces acting on the base of each slice are calculated using Eqs. (29) and (30), respectively.

## 9. Passive thrusts calculated considering locked-in stresses

In the preceding section it was shown that the passive

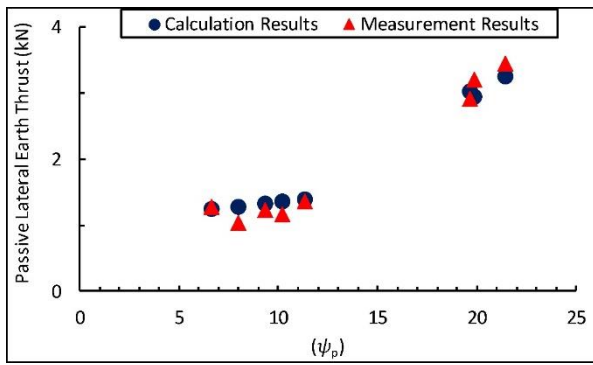


Fig. 11 The relationship between dilatancy angle and passive lateral earth thrusts according to calculation and measurement results obtained considering locked-in stresses

thrust magnitudes measured during the small scale retaining wall model tests and calculated using the method of slices with known strength parameters are compatible only for tests with pluviated backfill soils. However, when the model tests are conducted on compacted backfill soils, measured and calculated passive thrust magnitudes clearly differ (Fig. 9). In the previous section, it was hypothesized that the underlying cause of this discrepancy is the mechanical work that is elastically stored in soil grains during compaction. This is called locked-in stress. The validity of this hypothesis can be investigated using the results of the available model tests. For this purpose, magnitudes of  $I_\sigma$  for the bases of each slice for all tests were computed using Eq. (26) following the procedure explained in the previous section. Using these values in Eq. (25), passive lateral earth thrust magnitudes were recalculated. The results are compared with the measurements for all tests illustrated in Fig. 11. Clearly once the locked-in stresses are taken into consideration, the calculations and measurements agree with high accuracy for both pluviated and compacted backfills.

## 10. Discussion

The most important outcome of this study is that the sample preparation technique used for cohesionless soils directly influences the strength of the soil body as whole. When clean cohesionless soils are concerned, friction angle is the only strength parameter and its magnitude is dependent on mineralogy, grain shape, size distribution, stress state and density of packing. However, friction angle is not a function of overconsolidation ratio and it is not a function of loading and unloading cycles. Therefore method used for sample preparation does not affect the magnitude of  $\phi'_p$  as long as individual grains are not crushing. So, it is not possible to attribute the change in model backfill strength to the changes in  $\phi'_p$ . Model preparation technique can change the magnitude of  $\phi'_p$  only by varying the confining pressure and/or packing density. As the sole strength parameter is unaffected by the model preparation technique used (when models with same density and stress state are considered), then the increase in shearing resistance can only be attributed to the increase in

intergranular contact stresses above the value possible under self-weight stresses. This increase in intergranular contact stress is called locked-in stress (Rehman and Broms 1972, Sherif and Mackey 1977, Duncan and Seed 1986, Hanna and Al Khoury 2005, Hanna and Al-Romhein 2008) and it develops as a result of the mechanically stored work in elastic deformation of grains during compaction effort.

It is important to account for the presence of locked-in stresses in the design and construction of physical models. Especially when target soil density magnitudes can be achieved by compaction, tamping or any other mechanical effort, the influence of locked-in stresses must be considered in the analyses of results. Computed magnitudes of soil strength will be incorrect if they are based on vertical effective stresses that are functions of soil's unit weight and depth. Chen and Fang (2008) noted that both for pluviated and compacted soils vertical stresses are functions of depth and unit weight, however lateral earth pressures are affected by compaction. For calculating these residual lateral stresses, Mayne and Kulhawy (1982) collected data for different soils from literature and proposed an empirical method for calculating  $K_o$  of overconsolidated soils. However, this approach is practically difficult when compacted granular soils are concerned as relating compaction effort to overconsolidation ratio is problematic. On the other hand, Duncan and Seed (1986) suggested procedures for evaluating residual compaction induced lateral earth pressures that are based on an analytical hysteretic model. However, use of the procedure proposed by Duncan and Seed (1986) requires determination of post-compaction model parameters either by conducting tests or using empirical correlations. Therefore, it is important, and at the same time more practical to measure lateral pressures during model tests if compaction is used for model preparation. Otherwise, computed soil strength magnitudes will be incorrect.

On the other hand, it is considered unlikely that model preparation technique influences the geometries of the failure planes. Altunbas *et al.* (2017) observed that failure plane geometries in cohesionless soil bodies are functions of dilatant properties and Cinicioglu and Abadkon (2015) showed that frictional and dilatant properties are not influenced by induced overconsolidation. So it is not correct to suggest that compaction should be avoided in model preparation, however for all studies that use compaction, lateral stresses must be measured to be able to correctly understand and interpret the obtained results. Moreover, discussions and analyses of the results must be based on mean effective stresses, rather than vertical stresses or depth within model backfills. That requires the use of soil pressure measurements to track the actual magnitudes of stresses that are present in granular assemblies.

When it is attempted to calculate and consider locked-in stresses in model tests, it is vital to prevent soil arching during model preparation. Arching mechanism can mobilize when the model box is narrow relative to mean grain diameter of the testing material. Once arching occurs, actual stress distribution in the soil body will differ from the measurements. Therefore, it is imperative to rule out the possibility of arching by comparing the applied and

measured pressures at different depths.

The importance of the observations in this study extends to practical applications, as well as modelling studies. In the construction of retaining structures, when the design requires man-made backfills as in the case of cantilever gravity walls, the common practice requires compaction for improving the engineering properties of the backfill. Unfortunately, there is no dependable calculation method for relating the compaction effort to the increases in effective stresses. Therefore, it is prudent to measure the lateral earth pressure coefficient using load cells or in-situ tests, such as dilatometer or pressuremeter. As the results of this study shows, locked-in stresses calculated using Eq. (26) can be directly used in the analyses. Otherwise, the stresses and the strength that are used in design calculations will grossly deviate from the ones that are present in the field.

It is important to note that this study is conducted using small-scale models under 1 g conditions. Therefore, the stress levels employed in the model tests are well below the threshold that would cause individual grains to crush. Moreover, fill material used in the model tests is quartz sand. Accordingly, as a future study, it would be worthwhile to investigate locked-in stresses under the influences of elevated stress levels and using fill materials with different mineralogy.

## 11. Conclusions

The goal of this study is to investigate the influence of sample preparation method on physical model test results when cohesionless soils are concerned. For this purpose, several small scale physical retaining wall model tests were conducted under 1 g conditions. The physical models simulate passive backfill failure conditions, because deformations that lead to passive failure correspond to the problem during which the effects of model preparation technique employed is best preserved. Throughout the tests, changes in the stresses are measured using pressure transducers and the deformations of the soil body are tracked using PIV method. The results suggested that, for pluviated backfills, limit equilibrium method can be used to calculate passive thrust magnitude as long as the geometry of the failure surface and the strength parameters are known. The stresses in the soil body are calculated as a function of soil's unit weight. However, this is not sufficient whenever the backfill is prepared by compaction. As the results suggest, compaction effort induces locked-in stresses in the soil body increasing the frictional resistance, even though compaction changes neither the geometry of the failure surface nor the strength parameters. Accordingly, the results of this study indicates that it is necessary to use some method of soil stress measurement whenever compaction is used for backfill preparation, whether this is modelling study or construction work. Otherwise, computed stresses and resistances will grossly deviate from the actual values.

## Acknowledgements

The authors would like to thank The Scientific and

Research Council of Turkey (TUBITAK) for supporting this study with Project number 114M329.

## References

- Altunbas, A. (2014), "Influence of dilatancy on slip planes and on localization of strains", Ph.D. Dissertation; Bogazici University, Istanbul, Turkey.
- Altunbas, A., Soltanbeigi, B. and Cinicioglu, O. (2017), "Determination of active failure surface geometry for cohesionless backfills", *Geomech. Eng.*, **12**(6), 983-1001. <https://doi.org/10.12989/gae.2017.12.6.983>.
- Anil, Ö., Akbaş, S.O., Babagıray, S., Gel, A.C. and Durucan, C. (2017), "Experimental and finite element analyses of footings of varying shapes on sand", *Geomech. Eng.*, **12**(2), 223-238. <https://doi.org/10.12989/gae.2017.12.2.223>.
- Bolton, M.D. (1986), "The strength and dilatancy of sands", *Géotechnique*, **36**(1), 65-78.
- Broms, B. (1971), "Lateral earth pressure due to compaction of cohesionless soils", *Proceedings of the 4th International Conference on Soil Mechanics and Foundation Engineering*, Budapest, Hungary, October.
- Chakraborty, T. and Salgado, R. (2009), "Dilatancy and shear strength behavior of sand at low confining pressures", *Proceedings of the 17th International Conference on Soil Mechanics and Geotechnical Engineering: The Academia and Practice of Geotechnical Engineering*, Alexandria, Egypt, October.
- Chen, T.J. and Fang, Y.S. (2008), "Earth pressure due to vibratory compaction", *J. Geotech. Geoenviron. Eng.*, **134**(4), 437-444. [https://doi.org/10.1061/\(ASCE\)1090-0241\(2008\)134:4\(437\)](https://doi.org/10.1061/(ASCE)1090-0241(2008)134:4(437)).
- Cho, G.C., Dodds, J. and Santamarina, J.C. (2006), "Particle shape effects on packing density, stiffness, and strength: natural and crushed sands", *J. Geotech. Geoenviron. Eng.*, **132**(5), 591-602. [https://doi.org/10.1061/\(ASCE\)1090-0241\(2006\)132:5\(591\)](https://doi.org/10.1061/(ASCE)1090-0241(2006)132:5(591)).
- Cho, H.I., Sun, C.G., Kim, J.H. and Kim D.S. (2018), "OCR evaluation of cohesionless soil in centrifuge model using shear wave velocity", *Geomech. Eng.*, **15**(4), 987-995. <https://doi.org/10.12989/gae.2018.15.4.987>.
- Cinicioglu, O. and Abadkon, A. (2015), "Dilatancy and friction angles based on in situ soil conditions", *J. Geotech. Geoenviron. Eng.*, **141**(4), 06014019. [https://doi.org/10.1061/\(ASCE\)GT.1943-5606.0001272](https://doi.org/10.1061/(ASCE)GT.1943-5606.0001272).
- Duncan, J.M. and Seed, R.B. (1986), "Compaction-induced earth pressures under  $K_0$ -conditions", *J. Geotech. Eng.*, **112**(1), 1-22. [https://doi.org/10.1061/\(ASCE\)0733-9410\(1986\)112:1\(1\)](https://doi.org/10.1061/(ASCE)0733-9410(1986)112:1(1)).
- Fan, K. (1983), "Evaluation of the interslice side forces for lateral earth force and slope stability problems", M.Sc. Dissertation, University of Saskatchewan, Saskatchewan, Canada.
- Frost, J. and Park, J. (2003), "A critical assessment of the moist tamping technique", *Geotech. Test. J.*, **26**(1), 57-70. <https://doi.org/10.1520/GTJ11108J>.
- Hanna, A. (2001), "Determination of plane-strain shear strength of sand from the results of triaxial tests", *Can. Geotech. J.*, **38**(6), 1231-1240. <https://doi.org/10.1139/t01-064>.
- Hanna, A. and Al-Romhein, R. (2008), "At-rest earth pressure of overconsolidated cohesionless soil", *J. Geotech. Geoenviron. Eng.*, **134**(3), 408-412. [https://doi.org/10.1061/\(ASCE\)1090-0241\(2008\)134:3\(408\)](https://doi.org/10.1061/(ASCE)1090-0241(2008)134:3(408)).
- Hanna, A. and Al Khoury, I. (2005), "Passive earth pressure of overconsolidated cohesionless backfill", *J. Geotech. Geoenviron. Eng.*, **131**(8), 978-986. [https://doi.org/10.1061/\(ASCE\)1090-0241\(2005\)131:8\(978\)](https://doi.org/10.1061/(ASCE)1090-0241(2005)131:8(978)).
- Ingold, T.S. (1979), "The effects of compaction on retaining walls", *Géotechnique*, **29**(3), 265-283. <https://doi.org/10.1680/geot.1979.29.3.265>.

- Jaky, J. (1944), "The coefficient of earth pressure at rest (A nyugalmi nyomas tenyezaje)", *J. Soc. Hungarian Architect. Eng.*, **78**(22), 355-358. in Hungarian
- Kazemi, M. and Bolouri, J.B. (2018), "A curtain traveling pluviator to reconstitute large scale sand specimens", *Geomech. Eng.*, **14**(2), 131-139.  
<https://doi.org/10.12989/gae.2018.15.4.987>.
- Khatri, V.N., Debbarma, S.P., Dutta, R.K. and Mohanty, B. (2017), "Pressure-settlement behavior of square and rectangular skirted footings resting on sand", *Geomech. Eng.*, **12**(4), 689-705.  
<https://doi.org/10.12989/gae.2017.12.4.689>
- Kuo, C.Y. and Frost, J.D. (1996), "Uniformity evaluation of cohesionless specimens using digital image analysis", *J. Geotech. Eng.*, **122**(5), 390-396.  
[https://doi.org/10.1061/\(ASCE\)0733-9410\(1996\)122:5\(390\)](https://doi.org/10.1061/(ASCE)0733-9410(1996)122:5(390)).
- Ladd, R.S. (1974), "Specimen preparation and liquefaction of sands", *J. Geotech. Eng. Div.*, **100**(10), 1180-1184.
- Liu, S., Mao, H., Wang, Y.W. and Weng, L. (2018), "Experimental study on crushable coarse granular materials during monotonic simple shear tests", *Geomech. Eng.*, **15**(1), 687-694.  
<https://doi.org/10.12989/gae.2018.15.1.687>.
- Mayerhof, G.G. (1976), "Bearing capacity and settlement of pile foundations", *J. Geotech. Geoenviron. Eng.*, **102**(3), 195-228.
- Mayne, P.W. and Kulhawy, F.H. (1982), "K-OCR relationships in soil", *J. Geotech. Eng. Div.*, **108**(6), 851-872.
- Miura, S. and Toki, S. (1982), "A sample preparation method and its effect on static and cyclic deformation-strength properties of sand", *Soil. Found.*, **22**(1), 61-77.  
<https://doi.org/10.3208/sandf1972.22.61>.
- Nanda, S. and Patra, N.R. (2015), "Determination of soil properties for plane strain condition from the triaxial tests results", *Int. J. Numer. Anal. Meth. Geomech.*, **39**(9), 1014-1026. <https://doi.org/10.1002/nag.2337>.
- Oda, M. (1972), "The mechanism of fabric changes during compressional deformation of sand", *Soil. Found.*, **12**(2), 1-18.  
<https://doi.org/10.3208/sandf1972.12.1>.
- Potgieter, J.T. (2017), "Effects of compaction on lateral earth pressure", *Proceedings of the 6th International Young Geotechnical Engineers' Conference*, Seoul, Korea, September.
- Rahardjo, H. and Fredlund, D.G. (1984), "General limit equilibrium method for lateral earth force", *Can. Geotech. J.*, **21**(1), 166-175. <https://doi.org/10.1139/t84-013>.
- Rehman, S.E. and Broms, B.B. (1972), "Lateral pressures on basement wall: Results from full-scale tests", *Proceedings of 5th European Conference on Soil Mechanics and Foundation Engineering*, Madrid, Spain, April.
- Schanz, T. and Vermeer, P.A. (1996), "Angles of friction and dilatancy of sand", *Géotechnique*, **46**(1), 145-151.
- Sherif, M.M. and Mackey, R.D. (1977), "Pressures on retaining wall with repeated loading", *J. Geotech. Eng. Div.*, **103**(11), 1341-1345.
- White, D.J., Take, W.A. and Bolton, M.D. (2003), "Soil deformation measurement using particle image velocimetry (PIV) and photogrammetry", *Géotechnique*, **53**(7), 619-631.
- Wroth, C.P. (1972), "General theories of earth pressure and deformation", *Proceedings of the 5th European Conference on Soil Mechanics and Foundation Engineering*, Madrid, Spain, April.
- Zakerzadeh, N., Fredlund, D.G. and Pufahl, D.E. (1999), "Interslice force functions for computing active and passive earth force", *Can. Geotech. J.*, **36**(6), 1015-1029.  
<https://doi.org/10.1139/t99-065>.